DOI: 10.1002/cbic.200400420

Design, Synthesis and Biological Evaluation of Sugar-Derived Ras Inhibitors

Francesco Peri,*[a] Cristina Airoldi,[a] Sonia Colombo,[a] Enzo Martegani,[a] Anske Stephanie van Neuren,[b] Matthias Stein,[c] Chiara Marinzi,[a] and Francesco Nicotra[a]

The design and synthesis of novel Ras inhibitors with a bicyclic scaffold derived from the natural sugar D-arabinose are presented. Molecular modelling showed that these ligands can bind Ras by accommodating the aromatic moieties and the phenylhydroxylamino group in a cavity near the Switch II region of the protein. All the synthetic compounds were active in inhibiting nucleotide exchange on p21 human Ras in vitro, and two of them selectively inhibited Ras-dependent cell growth in vivo.

Introduction

Ras proteins are members of the superfamily of GTP-binding proteins and play an important role in signalling pathways that control cell growth and differentiation. They function as molecular switches by cycling between a GDP-bound inactive state and a GTP-bound active state. Human Ras exists in four different variants with an approximate molecular mass of 21 KDa. The first 165 of the 189 amino acid residues of the proteins show a high degree of sequence identity, but the rest of their sequences diverge.[1] Ras has been the subject of many pharmaceutical, genetic and biochemical studies.[2] Among the many results, it was found that the proto-oncogene that codes for Ras is mutated in about 20–30% of human tumours.[3] The oncogenic versions of Ras contain point mutations that block GTPase activity. This process in turn inhibits the cycling of the switch and leads to accumulation of the active form of Ras, thus contributing to tumour formation. Inhibition of the nucleotide-exchange process of mutated, tumourigenic Ras proteins therefore represents a potentially powerful strategy for preventing tumour formation and growth.

Traditional inhibitors designed for this purpose bear a guanine nucleotide residue or an analogue, but more recently a novel non-nucleotidic generation of Ras inhibitors that block the GDP–GTP exchange process has been developed in the Schering–Plough research institute.[4] Compounds **SCH-53870** and **SCH-54292** inhibited Ras activation with an activity in the lower μM range. The formation of tertiary complexes between the SCH inhibitors and Ras–GDP was observed by ESI mass analysis,[5] and, in the case of **SCH-54292**, a model of the tertiary complex was obtained by using NOE distances from NMR experiments.[6] This model places the naphthyl group of the ligand in a hydrophobic pocket in the vicinity of the critical Switch II region (residues 60–70). Both the Switch II and the Switch I regions (residues 30–37) undergo structural changes upon GTP binding and GTP hydrolysis. Furthermore, both switch regions are involved in the interaction with the guanine nucleotide-exchange factors (GEFs) and the GTPase-activating proteins (GAPs) that modulate Ras activity.[7] The model for the ligand–Ras–GDP complex showed that the sugar moiety of **SCH-54292** points out of the binding site and therefore does not appear to be crucial for the binding of the ligand with Ras. On the other hand, the hydroxylamine group seems to play an important role in the binding by being in close proximity to both the Mg^{2+} ion and the β-phosphate group of the bound GDP.

In this study, molecular modelling and virtual ligand docking were used in order to develop a new class of Ras inhibitors structurally related to the Schering–Plough inhibitors that could constitute similar ligand–Ras–GDP complexes. Here we present the chemical synthesis, in vitro and in vivo Ras inhibitor activity and the rationalisation of the binding modes of these compounds.

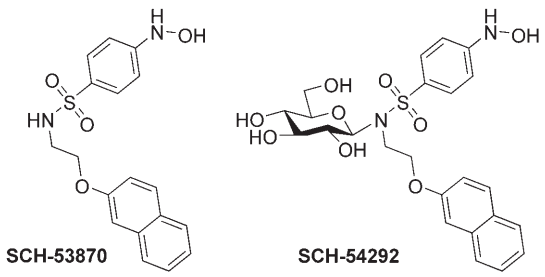

[a] *Dr. F. Peri, C. Airoldi, S. Colombo, E. Martegani, C. Marinzi, F. Nicotra*
Department of Biotechnology and Biosciences, University of Milano-Bicocca
Piazza della Scienza 2, 20126 Milano (Italy)
Fax: (+39) 026-448-3565
E-mail: francesco.peri@unimib.it

[b] *A. S. v. Neuren*
Anterio Consult & Research GmbH
Augustaanlage 26, 68165 Mannheim (Germany)

[c] *M. Stein*
Anterio Research GmbH
Augustaanlage 26, 68165 Mannheim (Germany)

Results and Discussion

Proof-of-concept: Docking of known binders

In order to validate the computational (docking) methodology, we initially investigated the interaction of the Schering–Plough inhibitors with Ras using the Glide program.[8] All of the known compounds docked well into the binding site in close proximity to the Switch II region. **SCH54292**, **SCH53239** and **SCH53870**, each bearing a naphthyl group, were oriented in the binding site in accordance with the experimentally derived NOE distances. The orientation of the inhibitors within the binding site was found to be similar to that described by Schering–Plough,[6] with the hydroxylamine group coordinating with both the bivalent Mg^{2+} ion and the β-phosphate of GDP, whereby an aromatic-charged interaction between the phenyl group and Lys16 is induced. The sugar moiety of **SCH-54292** and the guanine moiety of **SCH-53239** point out of the binding pocket and are not involved in significant interactions with the protein. However, we found important hydrogen-bond interactions not mentioned by the Schering–Plough research institute; namely between the sulfonamide group of the inhibitor and Gly10/Gly60, and between the hydroxylamine group of the ligand and Thr58 (Figure 1).

The interactions of the inhibitors' hydroxylamine groups with the magnesium ion and the β-phosphate of GDP are the main constituents of the binding enthalpy, and these interactions are therefore the major contributors to the GlideScore, which is an indication of the binding affinity for Ras.

Docking of novel structures

In the light of these encouraging results, the Glide program was applied to the in silico screening of novel inhibitors. Since the saccharidic moiety was shown not to interact with the protein, a series of structures lacking this residue was designed as potential new inhibitors. Compounds **1**–**4** present the putative pharmacophore groups covalently bound to a bicyclic core derived from the natural sugar D-arabinose (Scheme 1). The bicyclic moiety, whose synthesis from D-arabinose was developed by our group,[9] is a conformationally rigid scaffold, able to orient the pharmacophores (the hydroxylamino and the two aromatic groups) in a spatial arrangement potentially suitable for binding with the Ras–GDP complex. Compounds **1**–**4** fit well into the binding pocket, as observed by docking the molecules into the model of the Ras–GDP complex (Figure 2) and have very similar docking scores (Table 1). The two aromatic rings of the benzyl ethers on the bicyclic scaffold were expected to fill the hydrophobic pocket in an analogous way to the naphthalene groups of the Schering inhibitors. This is the case for only one of the aromatic rings, the second aromatic ring points out of the binding cavity (Figure 2). As expected, the phenyl group bearing the hydroxylamine is accommodated in the narrow pocket in close proximity to the Mg^{2+} ion, probably interacting with Lys16 through an aromatic-charge interaction. The hydroxylamino groups of all four compounds are

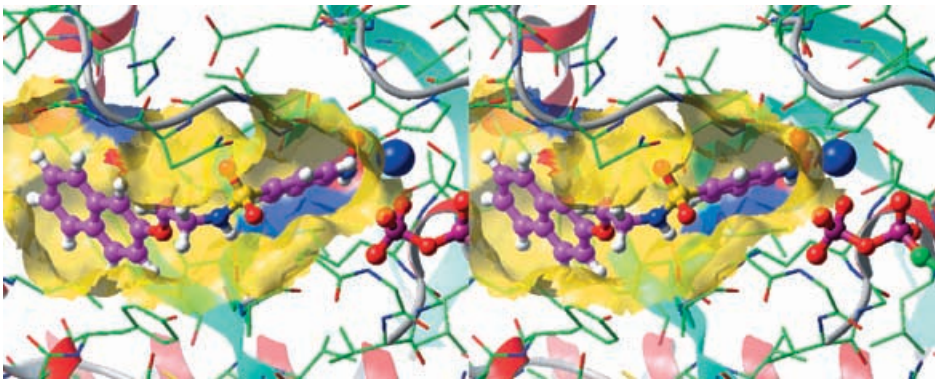

Figure 1. Stereoview of compound **SCH-53870** docked into the binding site of human p21 Ras.GDP; the molecular surface of the protein in close proximity to the ligand is coloured as follows: yellow for neutral residues, blue for positively charged residues and red for negatively charged residues. The Mg^{2+} ion is depicted as a blue CPK-model, and part of the GDP molecules is depicted as an atom-type coloured ball-and-stick model.

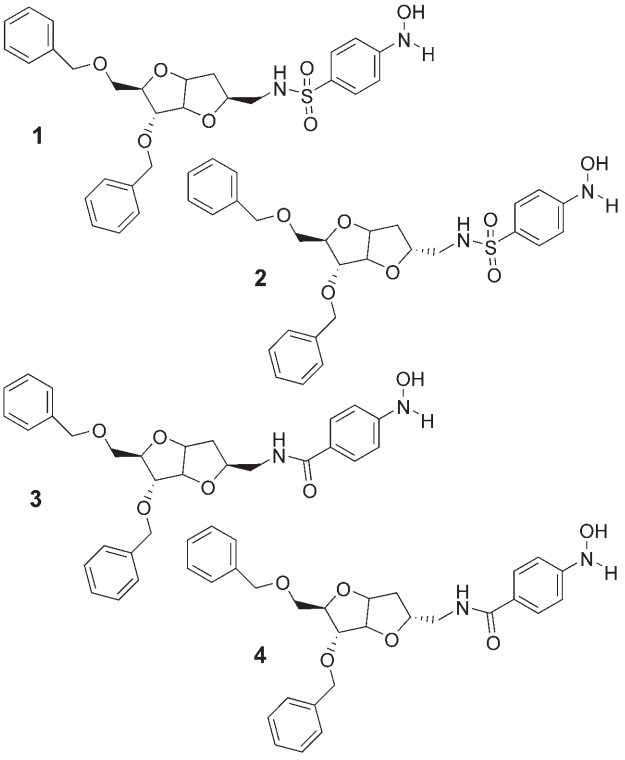

Scheme 1. Structures of compounds **1**–**4**; the hydroxylamino and phenyl pharmacophore groups are oriented in different ways depending upon the C-2 configuration of the bicycle.

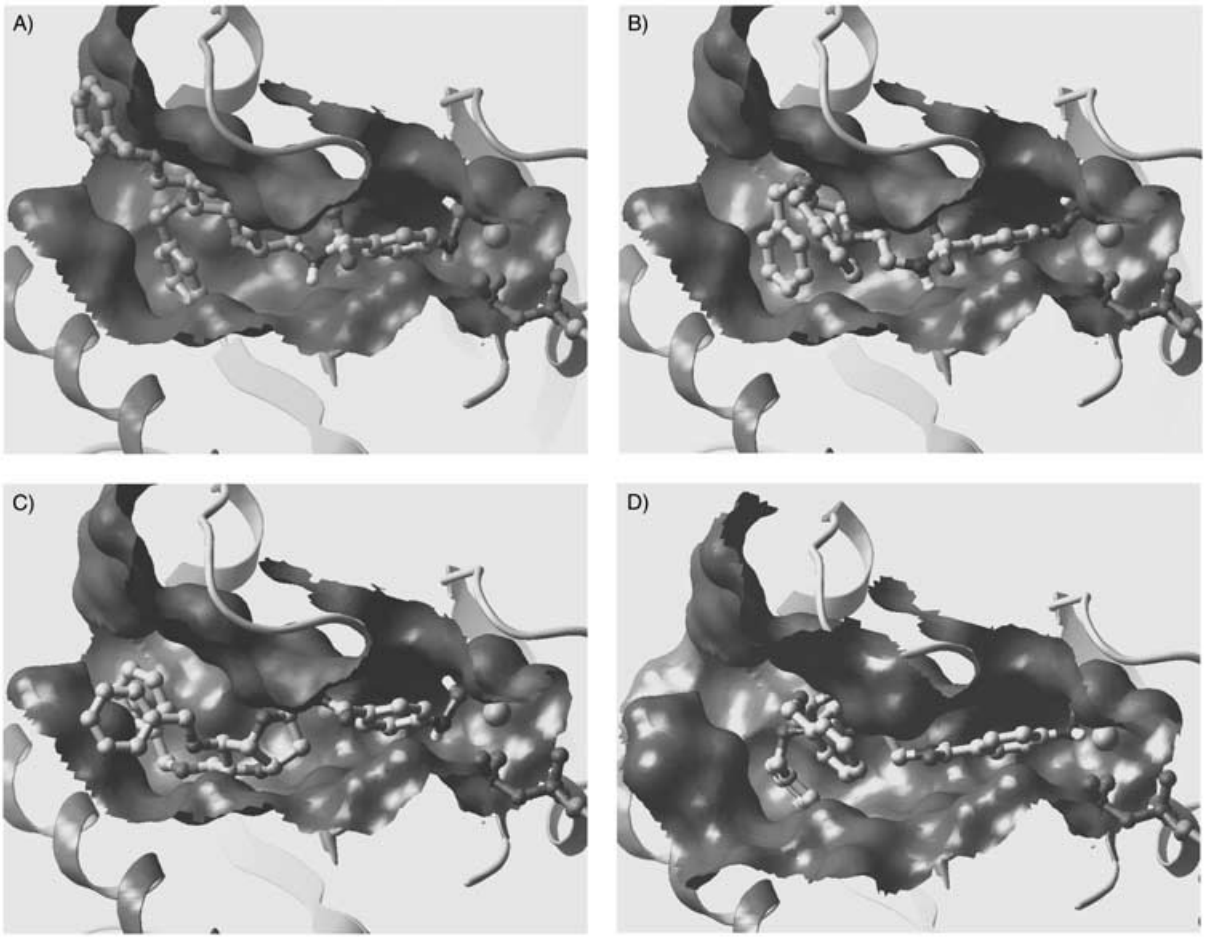

Figure 2. Docking of compounds A) **1**, B) **2**, C) **3** and D) **4** into the binding cavity of Ras.

Table 1. IC_{50} values and binding affinities for compounds **1**–**4** and **SCH-53870**.

Compound	IC_{50} [μM][a]	GlideScore	Percentage of top 40[b]
1	76.0 ± 1.4	−10.2	17%
2	57.3 ± 5.8	−9.9	25%
3	35.5 ± 0.7	−10.0	42%
4	62.3 ± 5.7	−10.1	15%
SCH-53870	56.0 ± 5.2	−8.9	

[a] Data represent the mean ± SD ($n = 3$). [b] For each of the four compounds, the 20 highest-scoring poses were selected, the 40 best scoring poses were selected from these 80 poses, and the recovery rate for each compound was calculated.

able to coordinate with both the bivalent Mg^{2+} ion and the β-phosphate of GDP, thus providing a strong polar interaction. Furthermore, in analogy with the binding model of the Schering–Plough compounds, the backbone carbonyl group of Thr58 is also an important potential hydrogen-bond-interaction partner for all four new compounds. In the modelled Ras–GDP-inhibitor complexes, the different configurations (*S* in **1** and **3**, *R* in **2** and **4**) of C-2 in the bicyclic cores and the different nature of the hydrogen-bond-forming groups (amide or sulfonamide) do not significantly influence the ligands' orientations within the binding pocket of Ras, neither are the ligands' predicted binding affinities (GlideScores) for Ras significantly different.

Chemical synthesis

Compounds **1**–**4** were prepared in parallel syntheses from the diastereomeric couple of precursors (*R*)-**5** and (*S*)-**5** with, respectively, *R* and *S* configuration at C-2. Both bicycles were obtained from D-arabinofuranose through the iodo-promoted cyclisation of allyl-C-glycoside, as described elsewhere.[9b] Bicyclic azides (*R*)-**5** and (*S*)-**5** were treated with triphenylphosphine in THF in the presence of 1% water to generate the corresponding amines (*R*)-**6** and (*S*)-**6** (Scheme 2), which were further treated with *p*-nitrobenzenesulfonyl chloride and triethylamine in dichloromethane to yield sulfonamides (*R*)-**8** and (*S*)-**8**, respectively. (*R*)-**6** and (*S*)-**6** were also condensed with *p*-nitrobenzoic acid in the presence of *N*-hydroxybenzotriazole (HOBt), diisopropylcarbodiimide (DIC) and diisopropylethylamine (DIPEA) to obtain *p*-nitrobenzenecarboxyamides (*R*)-**7** and (*S*)-**7**. Final reduction of the nitro groups with zinc and ammonium chloride in methanol generated the target compounds **1**–**4**. Compounds **1**–**4** were unstable in any organic

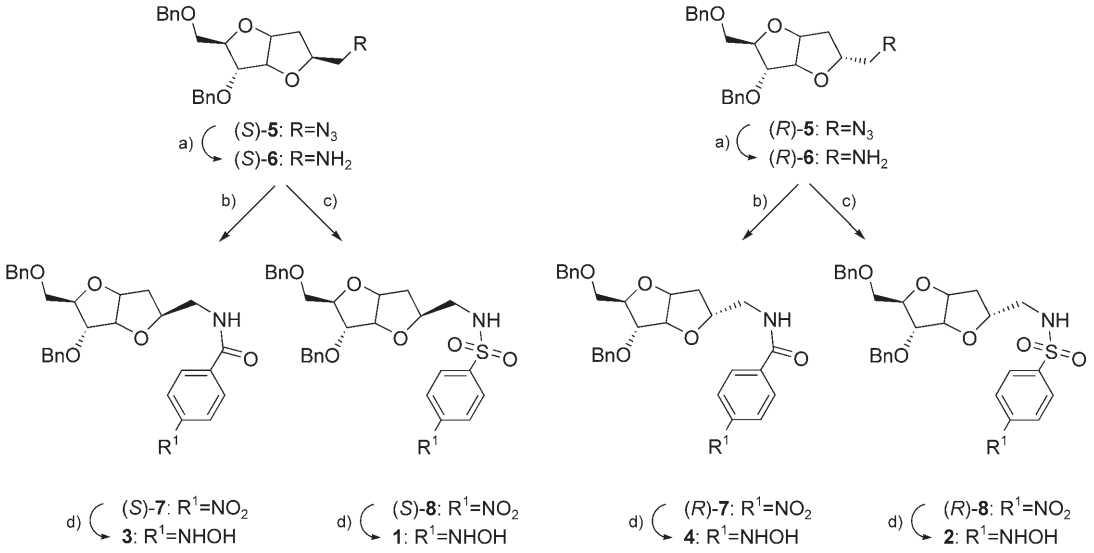

Scheme 2. Synthesis of bicyclic compounds **1**–**4**. a) PPh_3,THF, H_2O, 70 °C (75% for (*R*)-**6**, 96% for (*S*)-**6**); b) *p*-nitrobenzoic acid, HOBt, DIC, DIPEA, DMF (87% for (*R*)-**7**, 98% for (*S*)-**7**); c) *p*-nitrobenzenesulfonamide, Et_3N, CH_2Cl_2 (87% for (*R*)-**8**, 96% for (*S*)-**8**); d) Zn, NH_4Cl, MeOH (89% for **1**, 93% for **2**, 87% for **3**, 54% for **4**).

solvent as well as in water/DMSO mixtures at room temperature, and their oxidative degradation to the corresponding nitroso and azooxy derivatives is consistent with literature reports on hydroxylamine stability.[10] However, we did not observe significant degradation, as assessed by NMR analysis, after storage of compounds **1**–**4** as solids at −80 °C for months. In order to minimise oxidative degradation during inhibition assays, the bioactivity of these compounds was evaluated in the presence of dithiothreitol (DTT).

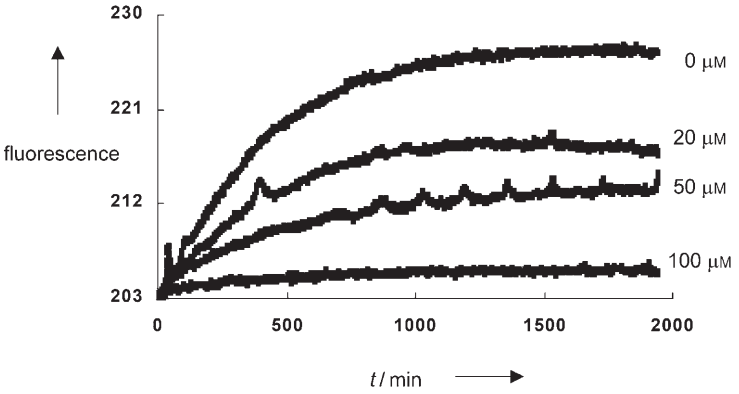

Figure 3. Cdc25^{mm}-stimulated nucleotide exchange on p21 h-Ras in the presence of increasing concentrations of **2**.

In vitro characterisation of Ras inhibitors

Compounds **1**–**4** were initially tested in vitro to investigate their ability to inhibit C-Cdc25^{mm}-stimulated nucleotide exchange on purified human Ras protein (p21 h-Ras). For this purpose a modified version of Lenzen's method was used.[11] The C-Cdc25^{mm}-stimulated guanine nucleotide exchange was monitored in the presence of an excess of the fluorescent 2′(3′)-*O*-(*N*-methylantraniloyl)-GTP (mant-GTP). p21 h-Ras was incubated with mant-GTP in the absence and in the presence of increasing concentrations of the putative inhibitors **1**–**4**. Compound **SCH-53870** was used as a positive control in the same experimental conditions. The exchange reaction was started by the addition of Cdc25.

The Cdc25-stimulated nucleotide exchange on p21 h-Ras in the presence of increasing concentrations (20 to 100 μM) of **2** is significantly inhibited in a dose-dependent manner in vitro (Figure 3).

IC_{50} values for compounds **1**–**4** and for **SCH-53870** (Table 1) are of the same order of magnitude, with **3** being slightly more potent than all the others. In vitro activities and docking scores of the bicyclic ligands suggest that they find analogous accommodation into the Ras cavity and thus have very similar binding orientation and affinity. For these reasons, further biological characterisation was performed only on compounds **2** and **4**, because of advantages in their preparation.[12]

On the other hand, a very significant difference between the behaviour of **2** and **4** in comparison with **SCH-53870** results from the analysis of kinetics of exchange, whereby an interesting inhibition of the fluorescent nucleotide binding is observed.[13]

The mechanism of action of the inhibitors was also investigated in a nucleotide-dissociation assay by measuring the release of fluorescent nucleotide by the Ras·mant-GDP complex in the presence of GDP and the exchange factor. A strong inhibition of guanine nucleotide release from Ras, and therefore a blocking of the exchange, was observed in the presence of **2** and **4** (Figure 4).

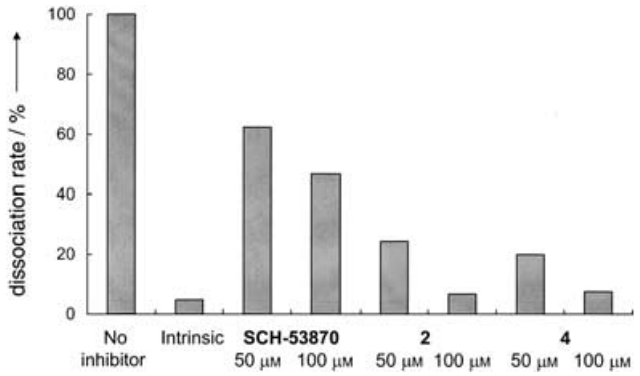

Figure 4. C-Cdc25^{mm}-stimulated dissociation of p21 h-Ras.mant-GDP complexes. The second column represents nucleotide dissociation due to Ras intrinsic GTPase activity. The values are expressed as a percentage of the control dissociation rate (5.4×10^{-3} s^{-1}).

In vivo characterisation of Ras inhibitors: Inhibition of yeast growth

It is well known that yeast cells have signal-transduction pathways that are similar to those of mammalian cells and many genes that are structurally and functionally homologous to human genes. On the other hand, yeast cells grow faster and present a simpler cellular organisation. The functional conservation between mammalian p21 Ras and yeast Ras proteins and the deep knowledge of the Ras-dependent processes in yeast offer the possibility of using *S. cerevisiae* as a model organism for studying Ras function and interactions with its modulators and/or inhibitors. Two homologues of mammalian p21 Ras, Ras1 and Ras2, have been identified in *S. cerevisiae*, and it has been demonstrated that these proteins are normally required for cell growth and proliferation.[14,15] Yeast Ras proteins are in fact key elements of a signal-transduction pathway that is involved in nutrient sensing and growth control. The main component of this pathway is adenylate cyclase, which catalyses the synthesis of cAMP. This molecule activates the cAMP-dependent protein kinase (PKA), an enzyme composed of catalytic subunits encoded by the *TPK1*, *TPK2* and *TPK3* genes, along with regulatory subunits encoded by the *BCY1* gene. The catalytic subunits phosphorylate substrate proteins involved in many important cellular processes, such as cell growth. In *S. cerevisiae*, adenylate cyclase activity is controlled by the Ras proteins.[14,15] Since these proteins are normally required for cell growth and proliferation, it is possible to test the in vivo activity of Ras inhibitors by monitoring their ability to inhibit or to reduce cell growth. Consequently, compounds **SCH-53870** and **1**–**4** were used to perform an inhibition test in a liquid medium on two different strains: a wild-type W303-1A and a *ras1*Δ, *ras2*Δ, *bcy1* strain. In this latter strain, the *bcy1* mutation bypasses the need of Ras for the cells to grow.[14] We expect a normal growth phenotype in such a strain (as in a wild-type without addition of inhibitors) if the inhibitor interacts selectively with the Ras proteins, while we expect inhibition or retardation of growth if the inhibitor interacts with other components involved in Ras-independent pathways. Therefore this strain allows the specificity of the inhibitors for the Ras/cAMP/PKA pathway to be tested. W303-1A and *ras1*Δ, *ras2*Δ, *bcy1* strains were grown until the early exponential phase. The cultures were then divided into aliquots: one aliquot was allowed to continue growing without addition of the inhibitor, while compounds **SCH-53870** and **1**–**4** were added to the other aliquots at a final concentration of 200 μM (Figure 5).

At different time points, a sample of culture was collected for cell-number determination. Addition of compounds **2**, **3** and **4** to a wild-type W303-1A strain completely inhibited cell growth, an almost complete inhibition was observed after addition of **SCH-53870**, while **1** was inactive (Figure 5A). On the other hand, only a small decrease in the cell growth was observed in strains *ras1*Δ, *ras2*Δ, *bcy1*, after addition of **2** and **4**, while **3** and **SCH-53870** were not very specific at this concentration. As expected, **1** was inactive (Figure 5C). Since all the

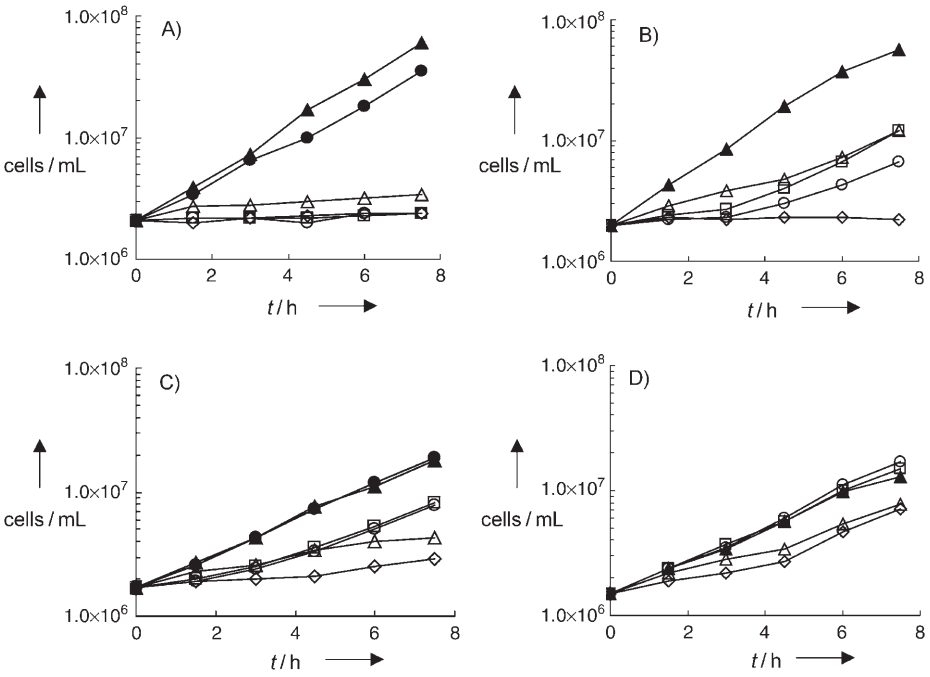

Figure 5. Inhibition test in liquid medium. W303-1A (A, B) and *ras1*Δ, *ras2*Δ, *bcy1* (C, D) cells were grown until the early exponential phase and then divided into aliquots: one aliquot was allowed to continue growing without addition of the inhibitor (▲), while molecules SCH-53870 (△), **1** (●), **2** (□), **3** (◇) and **4** (○) were added to the other aliquots at a final concentration of either 200 (A, C) or 50 μM (B, D). At different time points, a sample of culture was collected to determine the cell number.

arabinose-derived inhibitors (with the exception of **1**) completely inhibited cell growth at a concentration of 200 μM, the same inhibition tests were performed at a final inhibitors concentration of 50 μM (Figure 5B, D). Under these conditions, a reduction in cell growth was observed in strain W303-1A in the presence of **2**, **4** and **SCH-53870**, while a complete inhibition of cell growth was observed with **3**. These results are in agreement with the in vitro analysis, in which **2**, **4** and **SCH-53870** were observed to have a lower inhibitory capacity than **3**. When added to strain *ras1Δ, ras2Δ, bcy1*, **2** and **4** are inactive, while a small reduction in cell growth was observed after addition of **3** and SCH-53870.

These experiments on yeast cells suggest that our inhibitors specifically inhibit Ras-dependent growth, with compounds **2** and **4** giving the most significant results.

Effect of Ras inhibitor on mammalian cells

In order to investigate a specific effect on Ras-mediated signalling in vivo, inhibition of mammalian cell growth by compounds **2** and **4** was evaluated both in normal cells and in cells that had been transformed by k-Ras Arg12. Compounds **2** and **4** inhibit the growth of normal mouse fibroblasts NIH3T3 at a concentration of 100 μM; this effect was even more pronounced in k-Ras-transformed NIH3T3, here a complete arrest of growth is observed with **4** (Figure 6).

In order to verify that compounds **2** and **4** cause the in vivo inhibition of the Ras-mediated signalling, preliminary experiments were performed to measure the level of activation of MAPK after addition of the inhibitors to normal 3T3 fibroblasts growing in 10% serum. A pronounced decrease in phospho-MAPK expression was observed after 5 h at a final concentration of 50 μM; at 100 μM a stronger inhibition was observed (Figure 7).

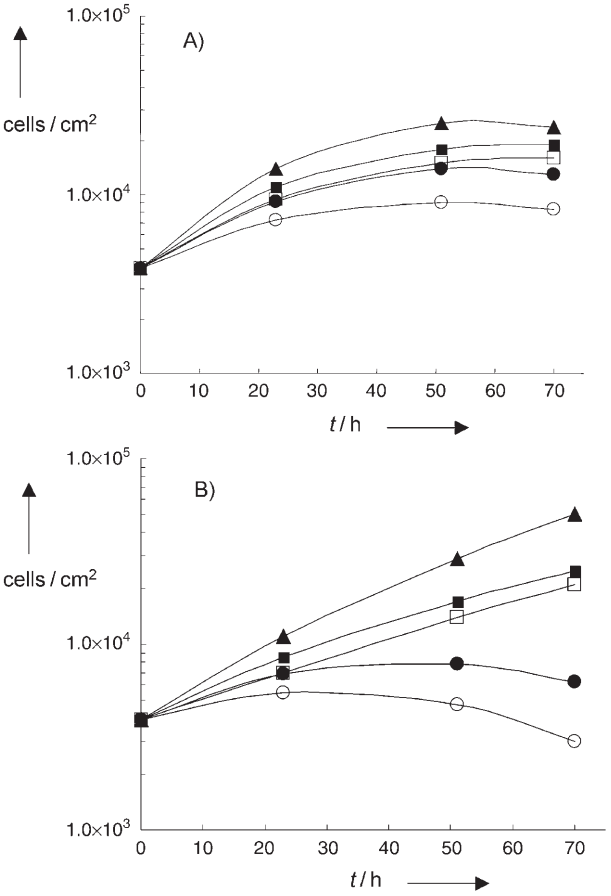

Figure 6. Inhibition test in mammalian cells. A) NIH3T3 and B) NIH3T3 k-Ras mouse fibroblasts were seeded into 60 mm dishes and grown for one day. Three dishes were allowed to continue growing without addition of inhibitor (▲), while **2** (squares) and molecule **4** (circles) were added to the other dishes at a final concentration of either 50 (black) or 100 μM (white). At different time points, sample cells were collected to determine the cell number.

Conclusion

Arabinose-derived bicyclic compounds **2** and **4** inhibit GTP association to Ras and GDP dissociation, as observed in vitro. Furthermore, compounds **2** and **4** are active in inhibiting cell growth in transformed mouse fibroblasts NIH3T3 with mutated Ras, and showed a specificity of action, having a negligible effect on Ras-independent *ras1Δ, ras2Δ, bcy1* yeast cell strains. Compound **1**, the least potent inhibitor in vitro, is completely inactive in inhibiting yeast cell growth in vivo. Compound **3** showed good activity in vitro, but low specificity and toxic effects in vivo. Inhibitors **2** and **4** have similar activity both in vitro and in vivo; this suggests that for C-2′ *R* isomers, the nature of the hydrogen-bond-forming groups (amide or sulfonamide) does not influence the binding affinity with Ras protein. On the other hand, quite a different behaviour is detected both in vitro and in vivo for **1** and **3**, which have C-2′ *S* configuration, but have, respectively, sulfonamide and amide functionalities. In this case, the nature of hydrogen-bond-forming group seems to dramatically influence the bioactivity.

The exact structure–activity relationship in these compounds is still under investigation.

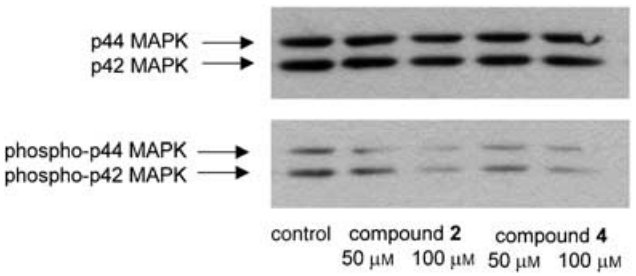

Figure 7. Assay of MAPK activation. Lysates (14 μg of total proteins) were separated by SDS-PAGE, transferred to nitrocellulose and immunodecorated with *anti*-p42/44 MAPK antibody and *anti*-phospho- p42/44 MAPK antibody.

The reported data show that this new class of compounds is able to selectively inhibit the activation of oncogenic Ras in mammalian cells, therefore representing a very promising target for development of novel anticancer drugs.

The antiproliferative and antitumoural effect of the described inhibitors is currently under investigation in vivo on animal models.

Experimental Section

Protein modelling: Before applying virtual ligand docking, the X-ray crystal structure of the Ras–GDP complex was optimised and prepared for the docking program. The X-ray structure of the human p21 h-Ras in its inactive form was taken from the Protein Data Bank (code: 4Q21) and optimised by applying the program Impact of Schrödinger and the OPLS-AA force field.[19] The protein was solvated in an explicit solvent box (65×65×65 ?) with 7991 water molecules and was allowed to relax slowly in several steps in order to orient the added hydrogens correctly and to relieve steric clashes. In the first optimisation step, force constraints were placed on all the heavy atoms of the protein, In the second step, the force constraints on the heavy atoms of the protein side chains were decreased in five substeps, but the constraints on the backbone atoms were kept constant, Then, in the third step, these force constraints on the backbone atoms of the protein were also decreased in five substeps, and finally, in the last step, no force constraints were applied and all the atoms of the system were flexible. Every step in this minimisation procedure was split into a steepest-descent step and a conjugate-gradient step; this is a general procedure within protein homology modelling. The protein structure obtained after this thorough minimisation procedure could be applied in the subsequent docking procedure.

The root-mean-square deviation of the minimised protein structure in comparison with the X-ray structure is 0.46 ? for the backbone atoms, 0.62 Å for the heavy atoms of the side chains and 0.55 Å for all protein heavy atoms.

Ligand modelling: In order to ensure the complete coverage of conformational space for the ligands, we applied a conformational search for each designed ligand using the Monte Carlo method (MCMM) implemented in the program MacroModel of Schrödinger. Random changes were made in the torsion angles during the search, and the OPLS-AA force field was used. The obtained conformations of the compounds were clustered with the program NMRCLUST,[20] in order to obtain the most representative conformations of the structures for the subsequent docking studies.

Ligand docking: The virtual ligand docking studies were performed with the Glide method implemented in the Impact program of Schrödinger. The model of the Ras–GDP complex was not modified further, as is recommended by Schrödinger, but all protein charged groups were kept charged and were not neutralised.

Glide requires the generation of an initial grid as a first step. The centre of the box enclosing this grid was defined by the Mg^{2+} ion, the β-phosphate group of the bound GDP and the two residues identified by NMR to be involved in interactions with the ligand: Arg68 and Leu100. The box dimensions were set to 26×26×26 Å. In the second step, the actual docking step, the dimensions of the box for placing the ligand centre were set to 12×12×12 Å, and the same centre was used as for the grid box. In this way, the complete cavity in close proximity to the Switch II region was included in the box where Glide would try to place the ligands. A scaling factor of 0.9 was applied to the van der Waals radii of protein and ligand atoms. The default values were applied for the other Glide parameters.

As a proof-of-concept, we first looked at the series of characterised compounds from the Schering–Plough research institute[4] in order to assess the validity of our computer-aided-design approach.

The poses depicted in Figure 1 were selected according to the same criteria as applied by Schafferhans et al.[21] When several docking solutions are suggested for each ligand, as is the case when several conformations of one ligand are docked, is it hard to discriminate efficiently between the solutions and to select the most relevant one. From several case studies done by Schafferhans et al., it can be seen that the best solution (the solution with the best score) is not always the one with the most similarity to the experimentally determined structure. However, if more than two ligands are considered, an optimal overall set of solutions for all ligands can be recognised by extracting those orientations that correspond to an optimal mutual similarity among the considered ligands. This additional criterion helps to select a set of relevant ligand placements, provided of course, that the ligands bind to the same binding site.

Furthermore, it can be analysed how often each of the four new designed compounds is recovered within the top scoring poses. For this purpose, the 20 highest-scoring poses of each compound were selected. Subsequently, the 40 highest-scoring poses of these 80 poses were selected, and the recovery rate for each compound (Table 1) was calculated.

Chemistry: All solvents were dried over molecular sieves (4 Å, Fluka), for at least 24 h prior to use. When dry conditions were required, the reactions were performed under Ar. Thin-layer chromatography (TLC) was performed on Silica Gel 60 F_{254} plates (Merck) with detection with UV light when possible, or charring with a solution containing conc. H_2SO_4/EtOH/H_2O (5:45:45) followed by heating at 180 °C. Column flash chromatography was performed on silica gel 230–400 mesh (Merck), with petroleum ether (40–60) as eluent. ^1H and ^{13}C NMR spectra were recorded at 400 MHz on a Varian MERCURY instrument at 300 K. Chemical shifts are reported in ppm downfield from TMS as internal standard, carbon and hydrogen numbering in bicyclic structures is shown in Scheme 3, aromatic carbons have been omitted in the description of the spectra.

Mass spectra were recorded on a MALDI2 Kompakt Kratos instrument, with gentisic acid (DHB) as matrix.

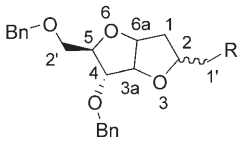

Scheme 3. Carbon and hydrogen numbering in bicycles.

Amines (*R*)-**6 and** (*S*)-**6**: Triphenylphosphine (525 mg, 2.02 mmol) was added to a solution of azide **5** (400 mg, 1.01 mmol) in THF/water (10:1; 44 mL), and the reaction mixture was stirred at 70 °C for 12 h. The solvents were evaporated, and the residue was purified by flash chromatography (AcOEt/MeOH 8:2–6:4) to give amines (*R*)-**6** (277 mg, 75 % yield) and (*S*)-**6** (354 mg, 96 % yield) as pale yellow oils .

(*R*)-**6**: ^1H NMR ($CDCl_3$): $\delta = 7.3–7.1$ (m, 10 H; H_{arom}), 4.74 (br t, 1 H; H-6a), 4.60–4.45 (2 ABq, 4 H; 2 CH_2Ph), 4.59 (m, 1 H; H-3a), 4.08 (m, 1 H; H-2), 4.00 (m, 1 H; H-5), 3.80 (dd, $J = 6.4$, 1.3 Hz, 1 H; H-4), 3.61 (dd, $J = 10.4$, 3.5 Hz, 1 H; H-2′a), 3.58 (dd, $J = 10.4$, 6.4 Hz, 1 H; H-2′b), 2.85 (dd, $J = 13.2$, 3.4 Hz, 1 H; H-1′a), 2.72 (dd, $J = 13.0$, 3.5 Hz, 1 H; H-1′b), 2.11 (dd, $J = 13.0$, 4.8 Hz, 1 H; H-1a), 1.60 (ddd, $J = 12.7$, 9.5, 4.7 Hz, 1 H; H-1b); ^{13}C NMR ($CDCl_3$): $\delta = 88.7$ (C-3a), 86.0 (C-4), 83.7 (C-6a), 83.4 (C-5), 80.3 (C-2), 73.7 (CH_2Ph), 72.3 (CH_2Ph), 70.5 (C-2′), 45.6 (C-1′), 36.3 (C-1); MS (MALDI-TOF): $m/z = 370.7$ $[M+H]^+$, 392.9 $[M+Na]^+$; elemental analysis calcd (%) for $C_{22}H_{27}NO_4$: C 71.52, H 7.37, N 3.79; found: C 71.51, H 7.40, N 3.71.

(*S*)-**6**: ^{1}H NMR ($CDCl_3$): $\delta = 7.40$–7.20 (m, 10H; H_{arom}), 4.70 (brt, $J =$ 4.5 Hz, 1H; H-6a), 4.63–4.50 (2ABq, 4H; 2CH_2Ph), 4.45 (m, 1H; H-3a), 4.06 (m, 2H; H-2, H-5), 3.88 (brd, $J = 5.7$ Hz, 1H; H-2), 3.62 (dd, $J = 10.3$, 3.9 Hz, 1H; H-2′a), 3.55 (dd, $J = 10.3$,6.0 Hz, 1H; H-2′b), 2.80 (m, 2H; H-1′a, H-1′b), 2.19 (m, 1H; H-1a), 1.89 (dd, $J = 13.8$, 5.4 Hz, 1H; H-1b); ^{13}C NMR ($CDCl_3$): $\delta = 89.2$ (C-3a), 85.1 (C-4), 85.0 (C-5), 84.0 (C-6a), 82.7 (C-2), 73.6 (CH_2Ph), 72.4 (CH_2Ph), 70.5 (C-2′), 46.7 (C-1′), 35.8 (C-1); MS (MALDI-TOF): $m/z = 371.3$ $[M+H]^+$, 393.3 $[M+Na]^+$; elemental analysis calcd (%) for $C_{22}H_{27}NO_4$: C 71.52, H 7.37, N 3.79; found: C 71.54, H 7.32, N 3.75.

Amides (*R*)-**7 and** (*S*)-**7**: Diisopropylamine (564 μL, 3.3 mmol), *N*-hydroxybenzotriazole (220 mg, 1.65 mmol), diisopropylcarbodiimide (260 μL, 1.65 mmol) and *p*-nitrobenzoic acid (220 mg, 1.3 mmol) were added to a solution of amine **6** (400 mg, 1.1 mmol) in DMF (30 mL). After the mixture had been stirred for 2 h at RT, the solvent was evaporated in vacuo, and the residue was purified by flash chromatography (gradient of polarity starting from petroleum ether/AcOEt 6:4). Amides (*R*)-**7** (496 mg, 87% yield) and (*S*)-**7** (558 mg, 98% yield) were obtained as yellow oils.

(*R*)-**7**: ^{1}H NMR ($CDCl_3$): $\delta = 8.23$, 7.92 (A_2X_2, 4H; H_{arom}), 7.4–7.2 (m, 10H; H_{arom}), 6.79 (brt, 1H; NH), 4.73 (brt, 1H; H-6a), 4.64–4.45 (2ABq, 4H; 2CH_2Ph), 4.52 (m, 1H; H-3a), 4.25 (m, 1H; H-2), 3.98 (m, 1H; H-5), 3.80 (brd, $J = 6.4$ Hz, 1H; H-4), 3.76 (m, 2H; H-1′a, H-2′a), 3.52–3.45 (m, 2H; H-1′b, H-2′b), 2.22 (dd, $J = 13.3$, 4.8 Hz, 1H; H-1a), 1.62 (ddd, $J = 13.3$, 10.4, 4.8 Hz, 1H; H-1b); ^{13}C NMR ($CDCl_3$): $\delta =$ 89.0 (C-3a), 85.8 (C-4), 83.5 (C-6a), 83.4 (C-5), 77.7 (C-2), 73.7 (CH_2Ph), 72.4 (CH_2Ph), 70.3 (C-2′), 43.3 (C-1′), 36.6 (C-1); MS (MALDI-TOF): $m/z = 502.9$ $[M-O+H]^+$, 518.4 $[M]^+$, 541.3 $[M+Na]^+$, 557.8 $[M+K]^+$; elemental analysis calcd (%) for $C_{29}H_{30}N_2O_7$: C 67.17, H 5.83, N 5.40; found: C 67.12, H 5.87, N 5.43.

(*S*)-**7**: ^{1}H NMR ($CDCl_3$): $\delta = 8.23$, 7.92 (A_2X_2, 4H; H_{arom}), 7.4–7.0 (m, 10H; H_{arom}), 7.40 (brd, 1H; NH), 4.69 (brt, 1H; H-6a), 4.64–4.45 (2ABq, 4H; 2CH_2Ph), 4.50 (m, 1H; H-3a), 4.0 (m, 1H; H-2), 4.05 (m, 2H; H-5, H-4), 3.77 (m, 2H; H-1′a, H-2′a), 3.40 (m, 2H; H-1′b, H-2′b), 2.22 (m, 1H; H-1a), 2.11 (dd, $J = 14.7$, 4.7, 1H; H-1b); ^{13}C NMR ($CDCl_3$): $\delta = 88.8$ (C-3a), 86.2 (C-4), 84.4 (C-6a), 83.5 (C-5), 78.5 (C-2), 73.4 (CH_2Ph), 72.7 (CH_2Ph), 68.8 (C-2′), 43.7 (C-1′), 33.5 (C-1); MS (MALDI-TOF): $m/z = 502.9$ $[M-O+H]^+$, 518.4 $[M]^+$, 541.3 $[M+Na]^+$, 557.8 $[M+K]^+$; elemental analysis calcd (%) for $C_{29}H_{30}N_2O_7$: C 67.17, H 5.83, N 5.40; found: C 67.19, H 5.81, N 5.38.

Sulfonamides (*R*)-**8 and** (*S*)-**8**. *p*-Nitrobenzenesulfonyl chloride (365 mg, 1.65 mmol) and triethylamine (230 μL, 1.65 mmol) were added to a solution of amine **6** (400 mg, 1.1 mmol) in dry dichloromethane (30 mL) at 0°C under argon atmosphere. The reaction mixture was allowed to warm to RT and stirred for 4 h. After this time, the solvent was evaporated, and the residue was purified by flash chromatography (increasing polarity of the eluent from petroleum ether/AcOEt 6:4). Sulfonamides (*R*)-**8** (530 mg, 87% yield) and (*S*)-**8** (585 mg, 96% yield) were obtained as yellow oils.

(*R*)-**8**. ^{1}H NMR ($CDCl_3$): $\delta = 8.30.$, 8.00 (A_2X_2, 4H; H_{arom}), 7.40–7.20 (m, 10H; H_{arom}), 5.25 (brt, $J = 6.0$ Hz, 1H; NH), 4.73 (brt, $J = 4.4$ Hz, 1H; H-6a), 4.60–4.40 (2ABq, 4H; 2CH_2Ph), 4.52 (m, 1H; H-3a), 4.12 (m, 1H; H-2), 3.97 (m, 1H; H-5), 3.71 (dd, $J = 6.5$, 1.3 Hz, 1H; H-4), 3.61 (dd, $J = 10.5$, 3.4 Hz, 1H; H-2′a), 3.50 (dd, $J = 10.4$, 6.2 Hz, 1H; H-2′b), 3.24 (ddd, $J = 12.8$, 5.7, 3.2 Hz, 1H; H-1′a), 3.0 (ddd, $J = 12.5$, 6.0, 6.0 Hz, 1H; H-1′b), 2.11 (dd, $J = 13.3$, 4.9 Hz, 1H; H-1a), 1.60 (ddd, $J = 13.5$, 10.5, 4.6 Hz, 1H; H-1b); ^{13}C NMR ($CDCl_3$): $\delta = 89.0$ (C-3a), 85.7 (C-4), 83.5 (C-6a), 83.4 (C-5), 77.0 (C-2), 73.7 (CH_2Ph), 72.4 (CH_2Ph), 70.2 (C-2′), 46.2 (C-1′), 36.0 (C-1); MS (MALDI-TOF): $m/z =$ 577.9 $[M+Na]^+$, 593.7 $[M+K]^+$; elemental analysis calcd (%) for $C_{28}H_{30}N_2O_8S$: C 60.64, H 5.45, N 5.05, S 5.78; found: C 60.62, H 5.48, N 5.01, S 5.72.

(*S*)-**8**. ^{1}H NMR ($CDCl_3$): $\delta = 8.19$, 7.95 (A_2X_2, 4H; H_{arom}), 7.44–7.20 (m, 10H; H_{arom}), 6.20 (m, 1H; NH), 4.62 (m, 1H; H-6a), 4.60–4.40 (2ABq, 4H; 2CH_2Ph), 4.39 (d, $J = 3.2$ Hz, 1H; H-3a), 4.24 (m, 1H; H-2), 4.10–4.00 (m, 2H; H-5, H-4), 3.79 (dd, $J = 10.6$, 2.3 Hz, 1H; H-2′a), 3.48 (dd, $J = 10.6$, 3.6 Hz, 1H; H-2′b), 3.19 (m, 1H; H-1′a), 3.09 (m, 1H; H-1′b), 2.17 (m, 1H; H-1a), 1.98 (dd, $J = 13.4$, 3.6 Hz, 1H; H-1b); ^{13}C NMR ($CDCl_3$): $\delta = 89.3$ (C-3a), 85.9 (C-4), 83.7 (C-6a), 83.6 (C-5), 78.8 (C-2), 73.4 (CH_2Ph), 72.6 (CH_2Ph), 69.4 (C-2′), 46.7 (C-1′), 34.0 (C-1); MS (MALDI-TOF): $m/z = 577.9$ $[M+Na]^+$, 593.7 $[M+K]^+$; elemental analysis calcd (%) for $C_{28}H_{30}N_2O_8S$: C 60.64, H 5.45, N 5.05, S 5.78; found: C 60.68, H 5.42, N 5.03, S 5.79.

Hydroxylamines 1–4: Zinc (143 mg, 2.2 mmol) and ammonium chloride (87 mg,1.65 mmol) were added to a solution of nitro derivatives **7** or **8** (1.1 mmol) in methanol (20 mL). The suspension was stirred for 40 min, then filtered on sintered glass with a celite layer, the solvent were evaporated, and the residue was purified by flash chromatography (increasing polarity of the eluent from petroleum ether/THF 6:4). Compounds **1** (529 mg, 89% yield), **2** (552 mg, 93% yield), **3** (482 mg, 87% yield) and **4** (300 mg, 54% yield) were obtained as oils.

Compound ***1***: ^{1}H NMR ($CDCl_3$): $\delta = 7.48$, 6.80 (A_2X_2, 4H; H_{arom}), 7.40–7.20 (m, 10H; H_{arom}), 5.45 (brt, $J = 5.4$ Hz, 1H; NH), 4.52 (m, 1H; H-6a), 4.60–4.40 (2ABq, 4H; 2CH_2Ph), 4.49 (m, 1H; H-3a), 4.19 (m, 1H; H-2), 4.01 (m, 1H; H-5), 3.83 (d, $J = 5.8$ Hz, 1H; H-4), 3.62 (dd, $J = 10.5$, 3.3 Hz, 1H; H-2′a), 3.42 (dd, $J = 10.5$, 5.4 Hz, 1H; H-2′b), 3.10 (m, 1H; H-1′a), 2.98 (m, 1H; H-1′b), 2.09 (m, 1H; H-1a), 1.90 (dd, $J = 13.5$, 4.6 Hz, 1H; H-1b); ^{13}C NMR ($CDCl_3$): $\delta = 89.4$ (C-3a), 85.4 (C-4), 84.5 (C-6a), 83.8 (C-5), 79.2 (C-2), 73.5 (CH_2Ph), 72.4 (CH_2Ph), 69.8 (C-2′), 46.9 (C-1′), 34.7 (C-1); MS (MALDI-TOF): $m/z =$ 563.6 $[M+Na]^+$, 579.5 $[M+K]^+$; elemental analysis calcd (%) for $C_{28}H_{32}N_2O_7S$: C 62.21, H 5.97, N 5.18, S 5.93; found: C 62.42, H 6.02, N 5.20, S 5.92.

Compound ***2***: ^{1}H NMR ($CDCl_3$): $\delta = 7.50$, 6.70 (A_2X_2, 4H; H_{arom}), 7.40–7.20 (m, 10H; H_{arom}), 4.61 (brt, $J = 4.6$ Hz, 1H; H-6a), 4.60–4.40 (2ABq, 4H; 2CH_2Ph), 4.42 (m, 1H; H-3a), 4.01 (m, 1H; H-2), 3.85 (m, 1H; H-5), 3.60 (dd, $J = 7.5$, 1.4 Hz, 1H; H-4), 3.51 (dd, $J = 10.4$, 3.6 Hz, 1H; H-2′a), 3.43 (dd, $J = 10.4$, 6.3 Hz, 1H; H-2′b), 3.09 (m, 1H; H-1′a), 2.85 (m, 1H; H-1′b), 1.99 (dd, $J = 13.6$, 5.1 Hz, 1H; H-1a), 1.60 (m, 1H; H-1b); ^{13}C NMR ($CDCl_3$): $\delta = 88.9$ (C-3a), 85.8 (C-4), 83.6 (C-6a), 83.3 (C-5), 77.1 (C-2), 73.7 (CH_2Ph), 72.4 (CH_2Ph), 70.2 (C-2′), 46.0 (C-1′), 36.0 (C-1); MS (MALDI-TOF): $m/z = 563.3$ $[M+Na]^+$, 579.1 $[M+K]^+$; elemental analysis calcd (%) for $C_{28}H_{32}N_2O_7S$: C 62.21, H 5.97, N 5.18, S 5.93; found: C 62.16, H 6.01, N 5.15, S 5.93.

Compound ***3***: ^{1}H NMR ([D_6]DMSO): $\delta = 8.66$ (brd, 1H; NHOH), 7.70 (brd, 1H; NHOH), 7.70–6.80 (A_2X_2, 4H; H_{arom}), 7.40–7.20 (m, 10H; H_{arom}), 5.47 (brd, 1H; NH), 4.56 (m, 1H; H-6a), 4.60–4.40 (2ABq, 4H; 2CH_2Ph), 4.47 (m, 1H; H-3a), 4.12 (m, 1H; H-2), 3.83 (m, 1H; H-5), 3.74 (dd, $J = 6.2$, 1.5 Hz, 1H; H-4), 3.60–3.30 (m, 4H; H-2′a, H-2′b, H-1′a, H-1′b), 2.03 (dd, $J = 13.3$, 4.9 Hz, 1H; H-1a), 1.60 (ddd, $J = 13.5$, 10.5, 4.6 Hz, 1H; H-1b); ^{13}C NMR ([D_6]DMSO): $\delta = 88.7$ (C-3a), 85.6 (C-4), 83.4(C-6a), 83.4 (C-5), 78.0 (C-2), 73.0 (CH_2Ph), 71.7 (CH_2Ph), 70.6 (C-2′), 42.6 (C-1′), 35.2 (C-1); MS (MALDI-TOF): $m/z = 505.2$ $[M+H]^+$, 527.1 $[M+Na]^+$, 543.3 $[M+K]^+$; elemental analysis calcd (%) for $C_{29}H_{32}N_2O_6$: C 69.03, H 6.39, N 5.55; found: C 69.07, H 6.41, N 5.56.

Compound ***4***: ^{1}H NMR ([D_6]DMSO): $\delta = 8.66$ (brs, 1H; NHO), 8.49 (brs, 1H; NOH), 7.70–6.80 (A_2X_2, 4H; H_{arom}), 7.30 (m, 10H; H_{arom}), 5.47 (brd, 1H; NH), 4.56 (m, 1H; H-6a), 4.46 (m, 1H; H-3a), 4.60–

4.40 (2 ABq, 4H; 2CH_2Ph), 4.12 (m, 1H; H-2), 3.83 (m, 1H; H-5), 3.74 (dd, J=6.2, 1.5 Hz, 1H;H-4), 3.60–3.30 (m, 4H; H-2′a, H-2′b, H-1′a, H-1′b), 2.01 (dd, J=13.3, 4.9 Hz, 1H; H-1a), 1.60 (m, 1H; H-1b); ^{13}C NMR ([D_6]DMSO): δ=88.2 (C-3a), 85.6 (C-4), 83.4(C-6a), 83.4 (C-5), 78.0 (C-2), 72.9 (CH_2Ph), 71.7 (CH_2Ph), 70.6 (C-2′), 41.5 (C-1′), 35.2 (C-1); MS(MALDI-TOF): m/z=505.5 [M+H]$^+$, 527.4 [M+Na]$^+$, 543.5 [M+K]$^+$; elemental analysis calcd (%) for $C_{29}H_{32}N_2O_6$: C 69.03, H 6.39, N, 5.55; found: C 69.02, H 6.37, N 5.53.

Expression and isolation of proteins: The C-Cdc25^{mm} (GEF from Mouse; portion of *CDC25*^{mm} that contains the catalytic domain of the protein)[16,17] was expressed in *Escherichia coli* by using the pGEX-2T expression vector and then affinity purified by using a Glutathione Sepharose 4B resin, while the p21 h-Ras was expressed in *E. coli* by using the pQE-30 expression vector and then affinity purified as a 6xHis-tagged protein by using a Ni-NTA resin.[17]

Measurement of C-Cdc25^{mm}-stimulated guanine nucleotide exchange on p21 h-Ras: To investigate the ability of putative Ras inhibitors to inhibit or to reduce the C-Cdc25^{mm}-stimulated nucleotide exchange on purified human Ras proteins, we used a technique described by Lenzen et al.[11] with some modifications. This approach utilises guanine nucleotides carrying an *N*-methylanthraniloyl fluorophore (MANT-GDP or MANT-GTP). p21 h-Ras (100 nM) and MANT-GTP (0.5 μM) were incubated in buffer A (50 mM Tris/HCl, pH 7.5, 1 mM $MgCl_2$, 100 mM NH_4Cl, 1 mM DTT) in the absence and presence of increasing concentrations of the putative inhibitors. The exchange reaction was started by the addition of C-Cdc25^{mm} (25 nM), then monitored at an excitation wavelength of 350 nm and emission wavelength of 450 nm with a Perkin–Elmer luminescence spectrometer. Measurements were taken every second. IC_{50} values were calculated from the slope of each curve.

Measurement of dissociation rate: We used the method described by Lenzen et al.[11] with some modifications to investigate the ability of Ras inhibitors to influence the C-Cdc25^{mm}-stimulated dissociation rate of p21 h-Ras·MANT-GDP complexes,. The complex p21 h-Ras·MANT-GDP (200 nM) and an excess of GDP (500 μM) were incubated in buffer B (40 mM Hepes, pH 7.5, 2 mM DTT, 100 μM $MgCl_2$) in the absence and presence of the inhibitors. The dissociation reaction was started by addition of C-Cdc25^{mm} (100 nM), then monitored at an excitation wavelength of 350 nm and emission wavelength of 450 nm with a Perkin–Elmer luminescence spectrometer. Measurements were taken every second. The slope of each curve was calculated by assuming a single exponential decay.

Yeast strains and growth conditions: The yeast strains used in this study were: W303-1A (*MATa leu2-3,112 ura3-1 trp1-92 his3-11,15 ade2-1 can1-100 GAL SUC mal*)[18] and T23-13B (*MATα his3, leu2, ura3, trp1, ras1ΔHIS3, ras2ΔURA3, bcy1*) (M. Wigler, Cold Spring Harbor Laboratory). Both strains were grown in 1% yeast extract, 2% bacto-peptone (YP) supplemented with 2% glucose and adenine (50 mg L^{-1}; YPDA). Growth was monitored by counting the cell number per mL with a Coulter counter.

Cell Cultures and growth conditions: NIH3T3- and NIH3T3-activated k-Ras (Arg12)[22] mouse fibroblasts (from Dr. P. Bossu, Dompé, L'Aquila, Italy) were grown in Dulbecco's modified Eagle's medium supplemented with 10% newborn calf serum (Gibco) (100 units per mL penicillin) and streptomycin (100 μg mL^{-1}). Cells were detached by treating them with 0.05% trypsin and EDTA (0.15 mM) and growth was monitored by counting the cell number per mL with a Coulter counter.

Assay of MAPK activation: Cells were scraped, and ice-cold Lysis buffer (25 m HEPES, pH 7.5, 150 mM NaCl, 1% NP-40, 0.25% Na deoxycholate, 10% glycerol, 25 mM NaF, 10 mM $MgCl_2$, 1 mM EDTA, 1 mM Na vanadate, one tablet of protease inhibitor mixture from Roche Applied Science in 50 mM of extraction medium) was added. The lysates were transferred to a microcentrifuge tube on ice and centrifuged. Proteins were separated by SDS-PAGE, transferred to nitrocellulose and immunodecorated with *anti*-p42/44 MAPK antibody and *anti*-phospho-p42/44 MAPK antibody (Cell Signalling Technology, Beverly, MA, USA). Bound antibodies were revealed by ECL Western blotting analysis system (Amersham Pharmacia Biotech).

Acknowledgements

This work was supported in part by the European Community's Human Potential Programme under contract HPRN-CT-2002-00173 (Glycidic Scaffolds), and in part by the FIRB (Design, preparation and biological evaluation of new organic molecules as potential innovative drugs). We thank Dr. Jörg Weiser for helpful discussions and reading the manuscript.

Keywords: ab initio calculations · antitumor agents · drug design · inhibitors · medicinal chemistry

[1] S. H. Kim, G. G. Privé, M. V. Milburn in *Handbook of Experimental Pharmacology, Vol. 108/1: GTPases in Biology* (Eds: B. F. Dickey, L. Birnbaumer), Springer, Berlin, **1993**, pp. 177–194.
[2] M. Paduch, F. Jelen, J. Otlewski, *Acta Biochim. Pol.* **2001**, *48*(4), 829–850.
[3] A. Wittinghofer, H. Waldmann, *Angew. Chem.* **2000**, *112*, 4360–4383; *Angew. Chem. Int. Ed.* **2000**, *39*, 4192–4214 and references cited therein.
[4] A. G. Taveras, S. W. Remiszewsky, R. J. Doll, D. Cesarz, E. C. Huang, P. Kirschmeier, B. N. Pramanik, M. E. Snow, Y.-S. Wang, J. D. del Rosario, B. Vibulbhan, B. B. Bauer, J. E. Brown, D. Carr, J. Catino, C. A. Evans, V. Girijavallabhan, L. Heimark, L. James, S. Liberles, C. Nash, L. Perkins, M. M. Senior, A. Tsarbopoulos, A. K. Ganguly, R. Aust, E. Brown, D. Delisle, S. Fuhrman, T. Hendrickson, C. Kissinger, R. Love, W. Sisson, E. Villafranca, S. E. Webber, *Bioorg. Med. Chem.* **1997**, *5*, 125–133.
[5] A. K. Ganguly, B. N. Pramanik, E. C. Huang, S. Liberles, L. Heimark, Y. H. Liu, A. Tsarbopoulos, R. J. Doll, A. G. Taveras, S. Remiszewski, M. E. Snow, Y. S. Wang, B. Vibulbhan, D. Cesarz, J. E. Brown, J. del Rosario, L. James, P. Kirschmeier, V. Girijavallabhan, *Bioorg. Med. Chem.* **1997**, *5*, 817–820.
[6] A. K. Ganguly, Y.-S. Wang, B. N. Pramanik, R. J. Doll, M. E. Snow, A. G. Taveras, S. Remiszewski, D. Cesarz, J. del Rosario, B. Vibulbhan, J. E. Brown, P. Kirschmeier, E. C. Huang, L. Heimark, A. Tsarbopoulos, V. M. Girijavallabhan, *Biochemistry* **1998**, *37*, 15631–15637.
[7] C. Herrmann, *Curr. Opin. Struct. Biol.* **2003**, *13*, 122–129.
[8] Glide 2.7, Schrödinger LLC, **2003**.
[9] a) F. Peri, L. Cipolla, B. La Ferla, F. Nicotra, *Chem. Commun.* **2000**, 2303–2304; b) F. Peri, R. Bassetti, E. Caneva, L. De Gioia, B. La Ferla, M. Presta, E. Tanghetti, F. Nicotra, *J. Chem. Soc. Perkin Trans. 1* **2002**, *5*, 638–644.
[10] a) S. Kazanis, R. A. McClelland, *J. Am. Chem. Soc.* **1992**, *114*, 3052–3059; b) C. Y. Wang, D. Zheng, J. B. Hughes, *Biotechnol. Lett.* **2000**, *22*, 15–19.
[11] C. Lenzen, R. H. Cool, A. Wittinghofer, *Methods Enzymol.* **1995**, *255*, 95–109.
[12] Diastereomers (*R*)-**5** and (*S*)-**5** were obtained by nucleophilic displacement on iodo-bicyclic precursors in a 4:1 ratio. Therefore compounds **2** and **4** were obtained in higher overall synthetic yields.
[13] S. Colombo, F. Peri, R. Tisi, F. Nicotra, E. Martegani, *Ann. N. Y. Acad. Sci.* **2004**, *1030*, 52–61.
[14] D. Broek, N. Samily, O. Fasano, A. Fujiyama, F. Tamanoi, J. Northup, M. Wigler, *Cell* **1985**, *41*: 763–769.
[15] J. M. Thevelein, J. H. de Winde, *Mol. Microbiol.* **1999**, *33*, 904–918.

[16] E. Martegani, M. Vanoni, R. Zippel, P. Coccetti, R. Brambilla, C. Ferrari, F. Sturani, L. Alberghina, *EMBO J.* **1992**, *11*, 2151 – 2157.
[17] P. Coccetti, L. Mauri, L. Alberghina, E. Martegani, A. Parmeggiani, *Biochem. Biophys. Res. Commun.* **1995**, *206*, 253 – 259.
[18] B. J. Thomas, R. Rothstein, *Cell* **1989**, *56*, 619 – 630.
[19] W. L. Jorgensen, D. S. Maxwell, J. Tirado-Rives, *J. Am. Chem. Soc.* **1996**, *118*, 11 225 – 11 236.
[20] A. Kelley, S. P. Gardner, M. J. Sutcliffe, *Protein Eng.* **1996**, *9*, 1063 – 1065.
[21] A. Schafferhans, G. Klebe, *J. Mol. Biol.* **2001**, *307*, 407 – 427.
[22] M. V. Milburn, L. Tong, A. M. de Vos, A. Brunger, Z. Yamaizumi, S. Nishimura, S. H. Kim, *Science* **1990**, *247*, 939 – 945.

Received: November 24, 2004
Revised: August 10, 2005

